Photochemical & Photobiological Sciences
https://doi.org/10.1007/s43630-024-00581-y

ORIGINAL PAPERS

Photodynamic inactivation of *E. coli* with cationic imidazolyl-porphyrin photosensitizers and their synergic combination with antimicrobial cinnamaldehyde

Madalena F. C. Silva[1] · Rafael T. Aroso[1] · Janusz M. Dabrowski[2] · Barbara Pucelik[3] · Agata Barzowska[3] · Gabriela J. da Silva[4] · Luis G. Arnaut[1] · Mariette M. Pereira[1]

Received: 3 January 2024 / Accepted: 18 April 2024

Abstract

Bacterial infections are a global health concern, particularly due to the increasing resistance of bacteria to antibiotics. Multi-drug resistance (MDR) is a considerable challenge, and novel approaches are needed to treat bacterial infections. Photodynamic inactivation (PDI) of microorganisms is increasingly recognized as an effective method to inactivate a broad spectrum of bacteria and overcome resistance mechanisms. This study presents the synthesis of a new cationic 5,15-di-imidazolyl porphyrin derivative and the impact of n-octanol/water partition coefficient (log*P*) values of this class of photosensitizers on PDI efficacy of *Escherichia coli*. The derivative with log*P* = –0.5, **IP-H-OH^{2+}**, achieved a remarkable 3 log CFU reduction of *E. coli* at 100 nM with only 1.36 J/cm^2 light dose at 415 nm, twice as effective as the second-best porphyrin **IP-H-Me^{2+}**, of log*P* = –1.35. We relate the rapid uptake of **IP-H-OH^{2+}** by *E. coli* to improved PDI and the very low uptake of a fluorinated derivative, **IP-H-CF$_3$$^{2+}$**, log*P* ≈ 1, to its poor performance. Combination of PDI with cinnamaldehyde, a major component of the cinnamon plant known to alter bacteria cell membranes, offered synergic inactivation of *E. coli* (7 log CFU reduction), using 50 nM of **IP-H-OH^{2+}** and just 1.36 J/cm^2 light dose. The success of combining PDI with this natural compound broadens the scope of therapies for MDR infections that do not add drug resistance. In vivo studies on a mouse model of wound infection showed the potential of cationic 5,15-di-imidazolyl porphyrins to treat clinically relevant infected wounds.

Graphical Abstract

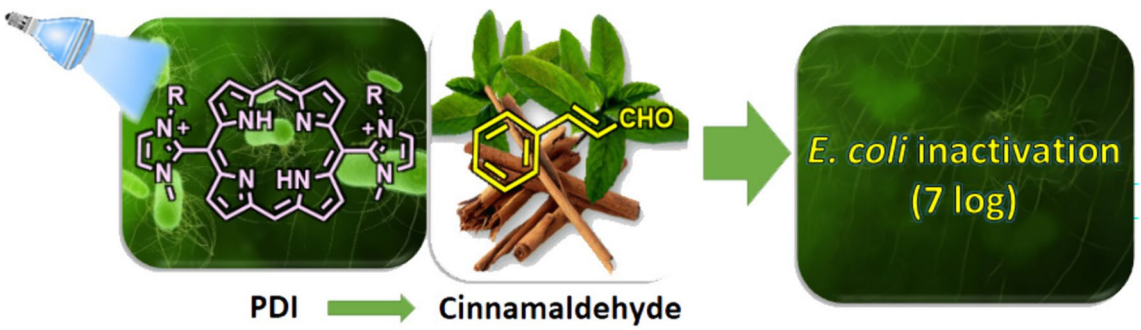

Keywords Photodynamic inactivation · *E. coli* · Cationic imidazolyl porphyrins · Photosensitizers · Dual therapy · Cinnamaldehyde

Extended author information available on the last page of the article

Published online: 12 May 2024

1 Introduction

Multi-drug resistant (MDR) bacterial infections are already responsible for approximately 1.3 million deaths each year. In particular, MDR *Escherichia coli* is mentioned in World Health Organization reports as one of the most troublesome microorganisms [1], causing up to 100,000 deaths annually [2]. Photodynamic inactivation (PDI), also named antimicrobial photodynamic therapy (aPDT), emerged as a viable alternative therapy to treat topical MDR bacterial infections due to its broad antimicrobial activity spectrum and low potential for developing resistance. PDI involves the use of a designed photosensitizing molecule, along with an appropriate light source and molecular oxygen, to generate reactive oxygen species (ROS) that can eliminate bacteria [3–6]. The clinical translation of PDI to photodisinfection of external wounds, such as diabetic foot ulcers, or of upper respiratory tract, ocular and buccal infections, is still limited by scientific challenges, namely, in the design and synthesis of photosensitizers at multigram scale, structural optimization to facilitate penetration of the double barrier present in Gram-negative bacteria, and effective infiltration in biofilms [7–9]. Studies with positively charged photosensitizers, such as cationic *meso*-(1-methylpyridinium-4-yl) [10–21] and *meso*-(4-*N,N,N*-trimethylammoniumphenyl) porphyrins [22–24], showed promising photoinactivation of *E. coli* and encouraged further work with cationic porphyrin derivatives.

Cationic imidazolyl-substituted photosensitizers, namely phthalocyanines and porphyrins, were successfully employed to photoinactivate Gram-negative bacteria such as *E. coli* [8, 25, 26]. Pereira, Dabrowski and co-workers showed that amphiphilic imidazole-phthalocyanines with 4 or 8 positive charges and 2 or 8 imidazolyl side chains effectively photo-inactivated *E. coli*. A phthalocyanine with 4 positive charges and a short chain (two carbon atoms) gave the best results: 7-log inactivation at a concentration of 100 nM and 10 J/cm^2 (white light irradiation) [25]. However, these imidazolyl phthalocyanines have problems of aggregation and solubility in aqueous solution, and our attention shifted to *meso* di- or tetra-imidazolyl porphyrins, which were also very effective in the photoinactivation of *E. coli* [8]. Furthermore, we also demonstrated that the size and number of charges are particularly relevant for the inactivation of *S. aureus* biofilms. A small size dicationic *meso*-imidazolyl porphyrin resulted in higher permeation through the polysaccharide polymer surface of biofilms, with consequent bacterial photoinactivation (7 log CFU reduction) with just 5.2 nM and 5 J/cm^2 [8]. Despite this progress, it is difficult to completely eradicate bacteria present in infected tissues and avoid recurrence with PDI alone [10, 27–32]. Recent studies emphasized that the synergic combination of PDI with existing antibiotics is a more promising approach to tackle multi-resistant bacteria and delay antibiotic resistance [26, 33, 34]. This approach enhances the efficacy of antibacterial treatments by leveraging the strengths of both PDI and antibiotics [27, 35–37]. We showed [26], in agreement with literature [34, 36], that the order and number of each individual treatment sessions impact the inactivation of MRSA or *E. coli*, and found that PDI followed by antibiotic administration yielded the best results.

Although the combination of PDI with antibiotics is probably the best approach to treat infections that extend beyond the surface accessible to illumination, the combination of PDI with other types of antimicrobials may be sufficient to treat a superficial localized infection. Natural antimicrobials with a low propensity to generate drug resistance are desirable for such combinations, especially if they are approved for human use as GRAS (Generally Recognized as Safe). This is the case with *trans*-cinnamaldehyde, a major component of the cinnamon plant, known for a broad range of antimicrobial activity against various strains of bacteria [38]. In human dermatological studies, the No-Observed-Adverse-Effect-Level (NOAEL) for cinnamaldehyde sensitization was set at 591 μg/cm^2 [39], which roughly corresponds to 0.5% content in a topical formulation. Several mechanisms may be involved in the antimicrobial effect of cinnamaldehyde, and their relevance may depend on the dosage. Although more research may be necessary to obtain an integrated view of its mechanism of action, there is a consensus that cinnamaldehyde alters the integrity of bacterial cell wall and their permeability [38, 40–42].

In this paper, we describe a pioneer study to evaluate the synergy of the combination of cinnamaldehyde with PDI in the photoinactivation of planktonic *E. coli*. The family of cationic di-imidazolyl-substituted porphyrin photosensitizers was expanded with a new member (**IP-H-OH^{2+}**) and structure–activity relations in PDI of planktonic *E. coli* were investigated. Preliminary studies in vivo show the feasibility of PDI with this class of photosensitizers.

2 Results and discussion

2.1 Synthesis

The dicationic *meso*-imidazolyl porphyrins were synthesized through alkylation of the commercially available 5,15-bis(1-methylimidazol-2-yl)porphyrin with different agents, which are expected to impart different degrees of hydrophilicity to the final products (Scheme 1). The 5,15-bis(1,3-dimethylimidazol-2-yl)porphyrinate diiodide (**IP-H-Me^{2+}**) and 5,15-bis(1-methyl-3-(3,3,3-trifluoropropyl)imidazol-2-yl)

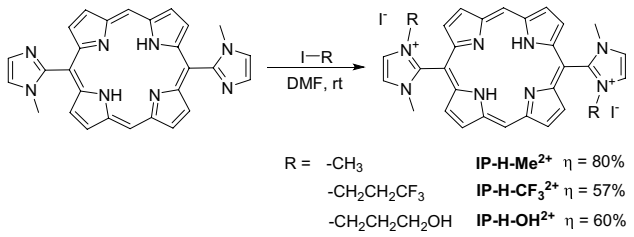

Scheme 1 Synthesis and structures of dicationic *meso*-imidazolyl porphyrins

porphyrinate diiodide (**IP-H-CF$_3$$^{2+}$**) were synthesized using our previously reported methodologies, being yields and characterization data in good agreement [8, 26, 43]. The synthesis of the new 5,15-bis(1-methyl-3-(3-hydroxypropyl) imidazol-2-yl)porphyrinate diiodide (**IP-H-OH^{2+}**) was carried out in DMF, under microwave irradiation (P_{max} = 125 W), at 100 ºC for 10 min, using iodopropanol as alkylating agent. The desired hydroxypropyl imidazolyl cationic porphyrin **IP-H-OH^{2+}** was precipitated from the crude with 2-methyltetrahydrofurane and was obtained in 60% isolated yield. It should be noted that the use of microwave irradiation to promote these alkylation reactions proved to be a better approach than conventional heating, giving the desired cationic imidazolyl porphyrin in just 10 min, instead of 24 h [8].

2.2 Photophysical and photochemical studies

The most relevant photophysical and photochemical properties of **IP-H-OH^{2+}** are summarized in Table 1 and compared with those of **IP-H-Me^{2+}** and **IP-H-CF$_3$$^{2+}$**, previously published [43]. Electronic absorption spectrum of **IP-H-OH^{2+}** in ethanol is typical of this class of compounds, exhibiting a Soret band at 400 nm, a $Q_y(0,1)$ band (λ = 499 nm); a $Q_y(0,0)$ band (536 nm); a $Q_x(0,1)$ band (576 nm) and a $Q_x(0,0)$ band (627 nm). This is consistent with the spectra of **IP-H-Me^{2+}** and **IP-H-CF$_3$$^{2+}$** [43]. The molar absorption coefficient of the Soret band of **IP-H-OH^{2+}** ($\varepsilon = 3.0 \times 10^5$ M^{-1} cm^{-1}) and its fluorescence quantum yield ($\phi_F = 0.11$) in ethanol are also comparable to the values of other cationic di-imidazolyl porphyrins. [43] The relatively low fluorescence quantum yields are consistent with those of other neutral and cationic 5,15-di-arylporphyrins [44].

The singlet oxygen quantum yield (Φ_Δ) is often used to evaluate the quality of a PDI photosensitizer. We determined Φ_Δ in ethanol and DMSO using time-dependent singlet oxygen phosphorescence emission at 1270 nm. Φ_Δ values of dicationic *meso*-imidazolyl porphyrins range between 0.27 and 0.63 in ethanol and 0.39 and 0.57 in DMSO, suggesting these are promising photosensitizers. These ranges agree with those of previously reported di-cationic porphyrins photosensitizers, such as 5,15-di[4-(3-*N,N,N*-trimethylammoniumpropoxy)phenyl]-10,20-di(4-trifluoromethylphenyl) porphyrin iodide ($\Phi_\Delta = 0.53 \pm 0.05$, in DMF) [45] and 5,15-di(1-methylpyridinium-4-yl)-10,20-diphenylporphyrin iodide ($\Phi_\Delta = 0.39$ in PBS) [46].

A parameter equally important in the characterization of a photosensitizer is its photostability [47, 48]. We determined the photodecomposition quantum yields (Φ_{pd}) of our dicationic *meso*-imidazolyl porphyrins (electronic absorption spectra in Figures S4-S6) and found that all these photosensitizers are very photostable, being **IP-H-OH^{2+}** the most promising (Table 1).

The *n*-octanol:water partition coefficient P_{OW}, or its logarithmic expression (log*P*), allows for a clear distinction between these photosensitizers. The propyl chain with a terminal CF_3 group appreciably increases the lipophilicity of **IP-H-CF$_3$$^{2+}$** (log*P* = 0.99) with respect to that of **IP-H-Me^{2+}** (log*P* = –1.35). This value is comparable to that of dicationic 5,15-diphenyl-10,20-di(1-methylpyridinium-4-yl)porphyrin diiodide (log*P* = 0.87), which possesses two N-methylpyridinium groups instead of the N-methylimidazolium groups, and two additional phenyl groups in the other *meso* positions [49]. Although **IP-H-OH^{2+}** has a hydrophilic functional group (OH) at the end of the alkyl chain, the longer size of this chain compensates for the

Table 1 Summary of photosensitizers' physicochemical properties

Porph	Log ε/M^{-1} cm^{-1} (λ/nm)[a]	Φ_F[a]	Φ_Δ	Φ_{pd}[c]	log*P*	Ref
IP-H-Me^{2+}	4.73 (395 nm); 3.66 (496 nm); 3.70 (532 nm); 3.34 (572 nm); 3.61 (625 nm)	0.092 ± 0.006	0.63 ± 0.05[a] (0.55 ± 0.04)[b]	(4.48 ± 0.38) × 10^{-5}	–1.35	[43]
IP-H-CF$_3$$^{2+}$	4.72 (395 nm); 3.54 (498 nm); 3.60 (533 nm); 3.18 (572 nm); 3.49 (626 nm)	0.17 ± 0.02	0.46 ± 0.03[a] (0.57 ± 0.03)[b]	(4.86 ± 0.30) × 10^{-5}	0.99	[43]
IP-H-OH^{2+}	4.48 (400 nm); 3.45 (499 nm); 3.48 (536 nm); 3.34 (576 nm); 3.28 (627 nm)	0.11 ± 0.01	0.27 ± 0.04[a] (0.39 ± 0.03)[b]	(2.77 ± 0.41) × 10^{-5}	–0.50	–

[a]In ethanol

[b]In DMSO

[c]In PBS

functional group and **IP-H-OH^{2+}** has an intermediate value of log*P* (log*P* = –0.50). This is in line with that of dicationic 5,15-di(*N*-(4-methoxybenzyl)-4-pyridyl)-10,20-di(4-pyridyl)porphyrin dichloride (log*P* = –0.52) [18]. Overall, the synthesized di-imidazolyl porphyrins allow us to investigate a series of relatively small-size dicationic photosensitizers that differ mostly in their *n*-octanol:water partition coefficients, to fine-tune the role of this factor in PDI efficacy.

2.3 Planktonic photodynamic inactivation

PDI of *E. coli* ATCC 25922 with dicationic *meso*-imidazolyl porphyrins was evaluated with a light dose of 1.36 J/cm^2 at 415 nm (Fig. 1). Remarkably, all these porphyrins enabled full inactivation of this Gram-negative bacterium at a concentration of 1 µM. Lowering the concentrations to 100 nM revealed differences between the photosensitizers. **IP-H-OH^{2+}** allowed for a 3 logs CFU reduction, **IP-H-Me^{2+}** for 2 logs and **IP-H-CF$_3$$^{2+}$** for 1 log reduction. This is consistent with our earlier work with **IP-H-Me^{2+}** [8]. The longer alkyl side chain ending in a haloalkyl functional group (CF_3) did not improve the photoinactivation of *E. coli* but the small alkyl chain with a more hydrophilic group (OH) did increase the photoinactivation of *E. coli*. The potency of **IP-H-Me^{2+}** at 100 nM and 1 µM with 1.36 J/cm^2 is comparable to that of **IP-Zn-Me^{2+}** at the same concentrations and 2 J/cm^2 [8]. Interestingly, Orlandi et al. demonstrated that 5,15-di(*N*-methyl-4-pyridyl)porphyrin has low *E. coli* inactivation in the µM range, which highlights the relevance of the type of cationic N-heterocyclic moiety in the overall photodynamic inactivation efficiency [20]. The activity of these pyridinium-derived porphyrins was improved with the introduction of more lipophilic groups in the porphyrin structure, such as benzyl [20] and phenoxyalkyl groups [13]. These results are in line with our findings, since the modulation of the lipophilicity of the dicationic *meso*-imidazolyl porphyrins described here also impacted their efficiency towards *E. coli* inactivation.

The positive charges of these imidazolyl porphyrins favor electrostatic interactions with the membranes of Gram-negative bacteria. When the interactions at the surface of the bacteria determine the efficacy of the treatment, triple washing with water is expected to reduce treatment efficacy. This washing was done to evaluate photoinactivation by photosensitizer molecules that diffused into the bacteria. Figure 2 shows that incubation with 100 nM concentrations followed by washing reduced photoactivation with **IP-H-Me^{2+}** and **IP-H-CF$_3$$^{2+}$** to non-significant levels, but ca. 3 log CFU reductions were achieved in incubations with 500 nM concentrations, and nearly 7 logs of inactivation were achieved at 1 µM. The observed decrease in photoinactivation efficiency after consecutive washing steps is in agreement with previous reports using other cationic porphyrins [45, 46]. Overall, this protocol confirms that **IP-H-OH^{2+}** is more potent at lower concentrations than the other two imidazolyl porphyrins, and suggests that it more rapidly partitions into inner regions of the bacteria. Moreover, the stronger photoinactivation before washings suggests that ROS generated in PDI with the photosensitizers on the surface of the bacteria can produce sufficient damage to inactivate bacteria.

2.4 Photosensitizer uptake

The uptake of photosensitizers by bacteria was studied with stock solutions of **IP-H-OH^{2+}** and **IP-H-Me^{2+}** in PBS:DMSO (DMSO 0.5%) and **IP-H-CF$_3$$^{2+}$** in PBS:THF (THF 0.5%). Porphyrin accumulation in planktonic bacteria was followed as a function of time, from 10 to 120 min of incubation, for 10 µM solutions, based on the fluorescence of porphyrins after their lyse with SDS 10% (Fig. 3). **IP-H-OH^{2+}** accumulation increases rapidly in the first 30 min and then stabilizes at ca. 2.4 × 10^5 molecules per cell. The uptake

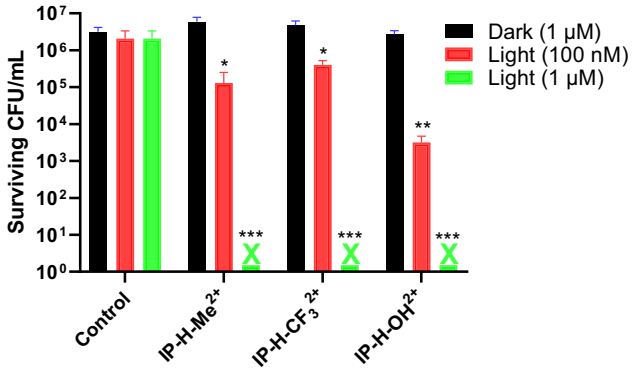

Fig. 1 Comparative *E. coli* photoinactivation studies using the *meso*-imidazolyl porphyrins and a 1.36 J/cm^2 light dose and 1 h incubation time. The labels * ($p < 0.05$), ** ($p < 0.01$) and *** ($p < 0.001$) represent statistical difference

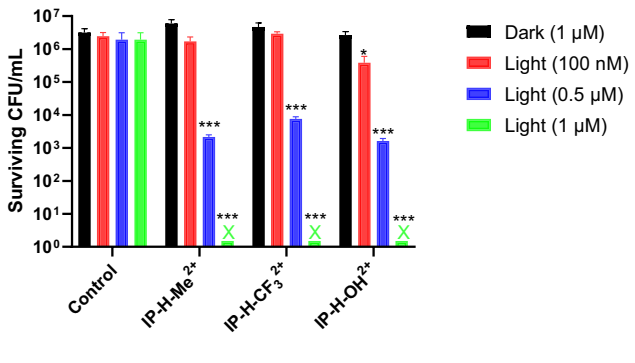

Fig. 2 Comparative *E. coli* photoinactivation studies using the synthesized *meso*-imidazolyl porphyrins and a 1.36 J/cm^2 light dose, after removing unbound PS with 3 × washings. The labels * ($p < 0.05$), ** ($p < 0.01$) and *** ($p < 0.001$) represent statistical difference relative to the control group

of **IP-H-Me^{2+}** is slower, reaching 1.9×10^5 molecules per cell after 2 h of incubation and may still increase further at longer times. Interestingly, **IP-H-CF$_3$$^{2+}$** uptake was much smaller. The difference in the stock solutions solvents may interfere with the uptake, but the most likely reason for the low uptake of **IP-H-CF$_3$$^{2+}$** is the unfavorable interaction between this lipophilic photosensitizer (log$P = 0.99$) and the negatively charged lipid A residues of the outer membrane of *E. coli* [3].

The differences in cell uptake were corroborated by flow cytometry and light scattering confocal microscopy (LSCM) studies, Figs. 4 and 5, respectively. The analysis of the histograms of the fluorescence intensities of the control bacteria (blue population), and bacteria with accumulated photosensitizer (red population) clearly demonstrates that **IP-H-Me^{2+}** and, particularly, **IP-H-OH^{2+}** have the highest cellular uptake. In addition, the LSCM representative pictures obtained for control cells (untreated bacteria, stained only with Hoechst33342) and each porphyrin also confirms the higher accumulation of **IP-H-Me^{2+}** and **IP-H-OH^{2+}** than **IP-H-CF$_3$$^{2+}$**.

The higher uptake of **IP-H-OH^{2+}** with 1 h of incubation is consistent with its enhanced PDI efficacy at low concentrations presented in Figs. 1 and 2. **IP-H-Me^{2+}** closely follows **IP-H-OH^{2+}** in cell uptake and PDI efficacy, and **IP-H-CF$_3$$^{2+}$** is the least successful photosensitizer in this family. It is possible that the performance of **IP-H-CF$_3$$^{2+}$** is limited by its lipophilicity. A moderate, but not excessive, hydrophilicity seems to be required for higher efficacy of photoinactivation of *E. coli* bacteria. **IP-H-OH^{2+}** combines both hydrogen-bond donors (OH) and positive charges in the photosensitizer structure.

2.5 PDI combined with cinnamaldehyde

Cinnamaldehyde is a natural antimicrobial agent whose mechanism of action is attributed to the disruption of bacterial membrane integrity [40]. Taking advantage of this membrane targeting mechanism and of the extensive uptake of membranes by **IP-H-OH^{2+}** and **IP-H-Me^{2+}**, we hypothesized that the administration of cinnamaldehyde after PDI may lead to a significant synergic effect. Thus, *E. coli* was incubated for 1 h with 50 nM of each photosensitizer concentration, in aqueous solution, and then irradiated with a 1.36 J/cm^2 light dose. Afterwards, cinnamaldehyde from a DMSO stock solution was added to the planktonic bacteria

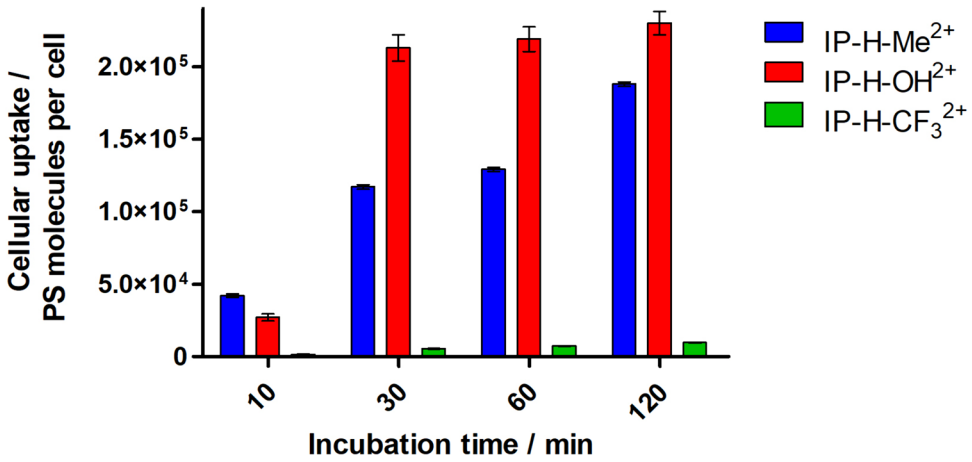

Fig. 3 Time-dependent cellular uptake of investigated porphyrins **IP-H-OH^{2+}**, **IP-H-Me^{2+}** and **IP-H-CF$_3$$^{2+}$** (with the initial 10 µM concentration) in *E. coli*

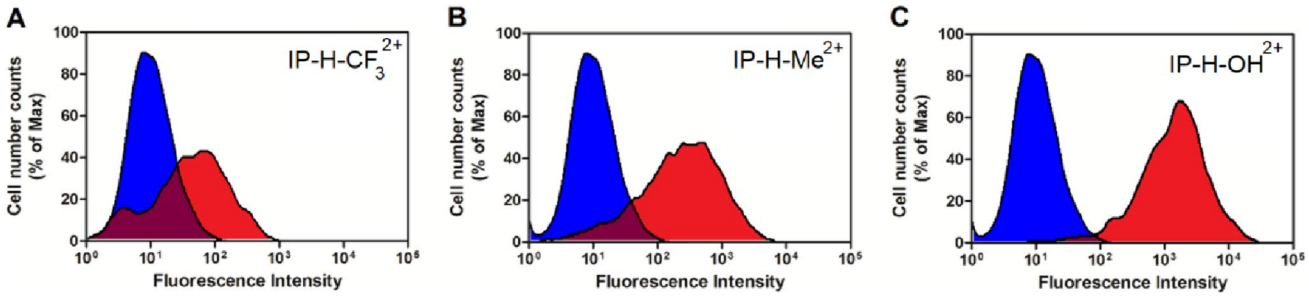

Fig. 4 Cellular uptake was determined in *E. coli* based on the red fluorescence of the selected porphyrin (**IP-H-CF$_3$$^{2+}$**, **IP-H-Me^{2+}**, **IP-H-OH^{2+}**) using flow cytometry equipped in red laser. Control bacteria are shown in blue

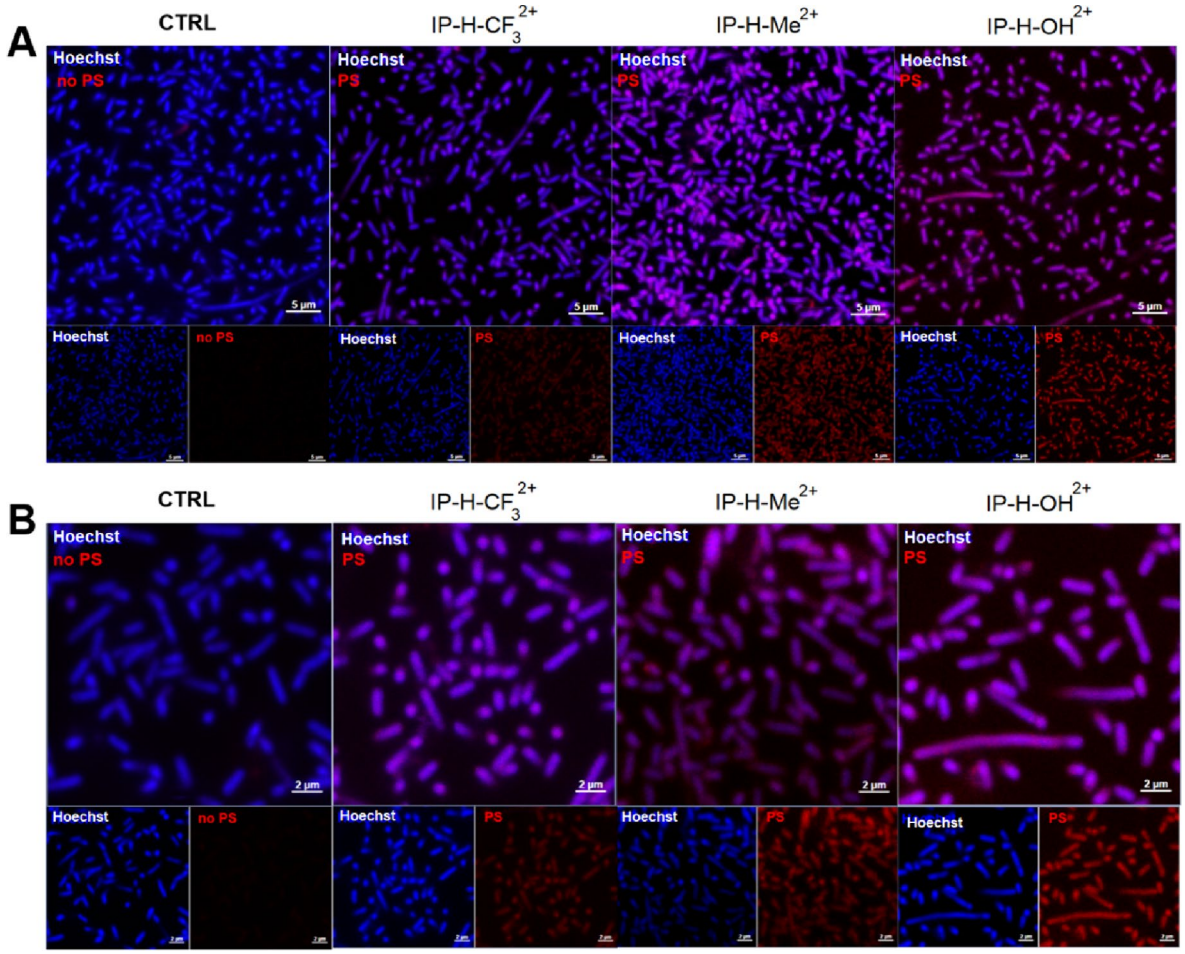

Fig. 5 Laser scanning confocal microscopy imaging of cellular uptake of **IP-H-OH**$^{2+}$, **IP-H-Me**$^{2+}$ and **IP-H-CF**$_3$$^{2+}$ in *E. coli* after 2 h of incubation: (A) with magnification × 100 (scale bar: 5 µm) and (B) confocal zoom (scale bar: 2 µm). The live cells were stained with Hoechst33342 (blue fluorescence); the accumulated porphyrin is indicated in red fluorescence

(7.5 mM final concentration, with 5% DMSO), followed by incubation in the dark for one additional hour, at room temperature. This concentration of cinnamaldehyde corresponds to ~ 0.1% of a topical formulation and is below the NOAEL for cinnamaldehyde sensitization. The results of the combination of **IP-H-Me**$^{2+}$ and **IP-H-OH**$^{2+}$ with cinnamaldehyde are presented in Fig. 6.

PDI with **IP-H-OH**$^{2+}$ at a concentration of 50 nM gives a modest 1.5 log CFU reduction, and with **IP-H-Me**$^{2+}$ the change in CFUs is not statistically significant. Interestingly, cinnamaldehyde alone at 7.5 mM also gives a 1.5 log CFU reduction. The antimicrobial activity of cinnamaldehyde is clearly evident with just 1 h of incubation at this non-toxic concentration. The combination of PDI with **IP-H-Me**$^{2+}$ followed by cinnamaldehyde administration gives a robust 3 log CFU reduction, while using **IP-H-OH**$^{2+}$ gives a remarkable 7 log CFU reduction. This is clear evidence of a synergy between the loss of integrity of the bacterial cell membrane

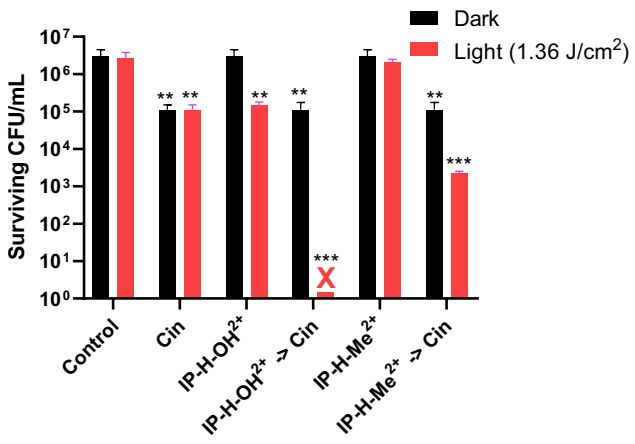

Fig. 6 Combination of 7.5 mM cinnamaldehyde (Cin) with PDI of *E. coli* using **IP-H-Me**$^{2+}$ and **IP-H-OH**$^{2+}$ as photosensitizers (50 nM; 1.36 J/cm^2 light dose). The labels ** ($p < 0.01$) and *** ($p < 0.001$) represent statistical difference relative to the control group

due to cinnamaldehyde and the facile uptake of **IP-H-OH^{2+}** by the cell membrane.

The sequence of the treatments, first PDI and then antimicrobial treatment with cinnamaldehyde, is in agreement with our previous experience of combining ciprofloxacin with PDI [26], which may be explained by the easy oxidation of cinnamaldehyde by the burst of oxidative damage produced by PDI [50, 51].

Cinnamaldehyde has antimicrobial activity but it is not an antibiotic, and it is not associated with drug resistance. The remarkable synergy between PDI with cinnamaldehyde treatments in the inactivation of *E. coli*, herein observed for the first time, is a notable example of how two treatments that do not contribute to bacterial resistance can be combined to inactivate bacteria at lower doses. The success of this combination may be attributed to the membrane damage caused by ROS produced in PDI [52], which potentiate the permeabilization of the bacteria membrane by cinnamaldehyde [53].

2.6 PDI in vivo

A preliminary in vivo study to assess the feasibility of treating local infections with PDI using dicationic 5,15-diimidazolyl porphyrins was conducted in Balb C mice with infected wounds. The backs of the mice were infected with a GFP-fluorescent *E. coli* to allow for quantitative and non-invasive follow-up of the infection (Fig. 7). After a single PDI treatment with **IP-H-Me^{2+}** at 25 μM and 120 J/cm^2 (420 nm light) light dose, a significant reduction of infection was observed over the 7 days follow-up after PDI. This is in stark contrast with the untreated control group, where a progressive increase of the infection area was observed over the same period. In vivo treatments require significantly higher photosensitizer concentration and light dose (~ 100-fold) than in vitro studies. This is expected because: (i) the interaction of photosensitizer molecules with the host cells reduces their accumulation in bacteria; (ii) the quenching of ROS by the host biomolecules reduces oxidative stress in the bacteria; (iii) absorption and scattering light by tissues lowers the light dose [10, 29–32]. In a PDI study with a comparable model of burn infection, treatment with 50 μM methylene blue and a light dose of 150 J/cm^2 (660 nm light) did not significantly reduce infection with respect to control [54]. That study showed that PDI with methylene blue was remarkably potentiated by the addition of 10 mM of KI. We obtained a reduction of the infection with **IP-H-Me^{2+}**–PDI alone. We expect that further studies will show that cinnamaldehyde can offer a potentiation comparable to that of KI, although using different mechanisms, and contribute to make PDI a more valuable alternative to treat superficial infections without aggravating drug resistance.

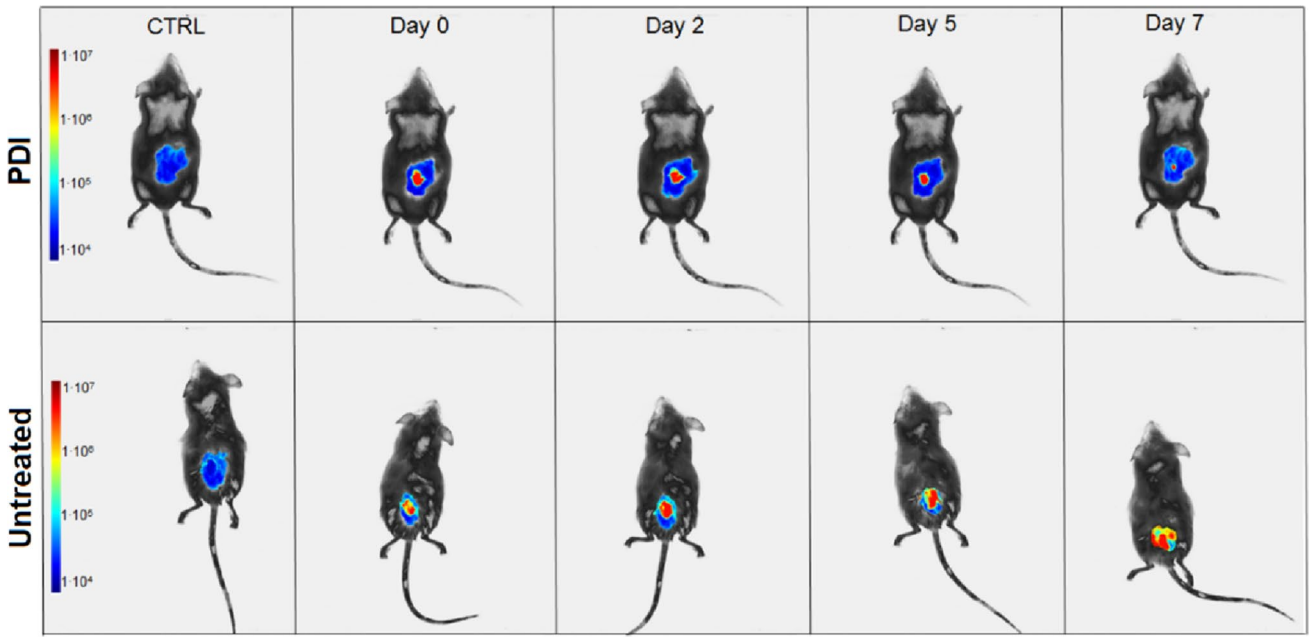

Fig. 7 Photographs of mice with excision wounds infected with *E. coli*. Panel of representative fluorescent images showing response to PDI on different days post-treatment. PDI was performed using 25 μM of **IP-H-Me^{2+}** and 120 J/cm^2 blue light (420 nm)

3 Conclusion

We synthesized a new dicationic 5,15-di-imidazolyl porphyrin (**IP-H-OH^{2+}**), in just 10 min reaction time, using microwave irradiation, with 60% yield, to expand the family of cationic imidazolyl photosensitizers and investigate structure–activity relations in PDI of *E. coli*. **IP-H-OH^{2+}** (log*P* = – 0.50) has half the singlet oxygen quantum yield and twice the photostability of **IP-H-Me^{2+}** (log*P* = –1.35). **IP-H-CF$_3$$^{2+}$** (log*P* = 0.99) has an intermediate Φ_Δ and a stability similar to **IP-H-Me^{2+}**. Considering that lower Φ_Δ and high photostability tend to compensate each other, these photosensitizer differ mostly in their octanol:water partition coefficients. All of them reduced planktonic *E. coli* CFUs by ~ 7 log units at 1 μM concentrations with 1.36 J/cm^2 (415 nm light), which reveals that this class of photosensitizers is remarkably efficient in PDI of planktonic bacteria. At 100 nM, **IP-H-OH^{2+}** became the most potent photosensitizer, followed by **IP-H-Me^{2+}**. **IP-H-OH^{2+}** has a faster uptake in *E. coli* than **IP-H-Me^{2+}**, and **IP-H-CF$_3$$^{2+}$** showed the lowest uptake. The high affinity of **IP-H-OH^{2+}** for the bacterial membrane is likely the reason for its enhanced photodynamic efficacy.

The strong interaction of **IP-H-OH^{2+}** with bacterial membranes is consistent with the success found in its combination with cinnamaldehyde to inactivate *E. coli*. This natural antimicrobial agent is known to disrupt the bacterial membrane, and the addition of 7.5 mM of cinnamaldehyde to *E. coli* shortly after PDI with 100 nM **IP-H-OH^{2+}** afforded a dramatic photoinactivation of 7 log CFUs. Cinnamaldehyde is widely used in the food industry and as a fragrance ingredient. Its combination with photosensitizers to treat superficial infections has a very favorable safety profile and can enhance PDI efficacy.

Preliminary in vivo studies of PDI with 25 μM **IP-H-Me^{2+}** showed the feasibility of using this class of molecules to treat infected wounds when a light dose of 120 J/cm^2 is delivered 30 min after the addition of the photosensitizer to the wound. Light doses of this magnitude can be delivered in 12 min without thermal effects. These treatments can be repeated without generating drug resistance. Translation to clinical applications will benefit from more efficient treatments performed in shorter times. Combination therapies, namely with cinnamaldehyde, may contribute to shorten the treatment time and increase the efficacy of PDI. We hope that topical formulations with potent photosensitizers like **IP-H-OH^{2+}** combined with antimicrobial agents will be developed to change the management of localized, superficial infections and minimize the propagation of multidrug-resistant bacteria.

4 Experimental procedures

4.1 Synthesis

All reagents and solvents were purchased from commercial sources and used without further purification. 5,15-bis(1-methylimidazol-2-yl)porphyrin was acquired from PorphyChem. 5,15-bis(1,3-dimethylimidazol-2-yl)porphyrinate diiodide (**IP-H-Me^{2+}**) and 5,15-bis(1-methyl-3-(3,3,3-trifluoropropyl)imidazol-2-yl)porphyrinate diiodide (**IP-H-CF$_3$$^{2+}$**) were synthesized as previously reported [43]. Electronic absorption spectra were recorded on a Shimadzu 2100 spectrophotometer. Nuclear magnetic resonance ^{1}H spectra were recorded on a 400 Bruker Avance spectrometer (400 MHz), using tetramethylsilane (δ = 0.00 ppm) as internal standard. The high-resolution mass spectrometry (HRMS) analysis was carried out using a Bruker Microtof.

4.1.1 5,15-bis(1-methyl-3-(3-hydroxypropyl)imidazol-2-yl) porphyrinate diiodide (IP-H-OH^{2+})

In a 5 mL microwave vial, the 5,15-bis(1-methylimidazol-2-yl)porphyrin (30 mg, 0.064 mmol) was dissolved in DMF (0.2 mL) and 3-iodopropanol (0.2 mL, 0.32 mmol) were added. The reaction was carried out under microwave irradiation with P_{max} = 125 W, at 100 ºC for 10 min. After reaction completion, the solvent was evaporated and the crude was redissolved in a minimum amount of methanol. The product was precipitated following the addition of 2-methyltetrahydrofurane to the methanolic solution, affording a dark purple solid after filtration (23 mg, 60% yield). ^{1}H NMR (400 MHz, CD_3OD) δ, ppm: mixture of atropisomers 10.89 (s, 2H), 9.86 (br s, 4H), 9.18 (br s, 4H), 8.48 (s, 2H), 8.41 (s, 2H), 4.25–4.23 (m, 4H), 3.86–3.84 (m, 6H), 3.69–3.66 (m, 4H), 1.82–1.81 (m, 4H); ESI–MS m/z: obtained 587.2858 $[M\text{-}2I\text{-}H]^+$; calculated for $[C_{34}H_{35}N_8O_2]^{.+}$ 587.2877. See characterization spectra in Figs. S1 and S2.

4.2 Photophysical and photochemical studies

4.2.1 Fluorescence quantum yield

Fluorescence spectra were obtained in obtained in a Horiba Jobin Yvon—Spex Fluorolog 3.22. The determination of the fluorescence quantum yields (Φ_F) was conducted in ethanol using a comparative method, according to Eq. (1):

$$\Phi_F = \Phi_F{}^{Std}\frac{FA_{Std}\eta^2}{F_{Std}A\eta_{Std}{}^2} \quad (1)$$

where F and F_{Std} are the integrals of the fluorescence emission curves of the samples and the standard, respectively; A and A_{Std} are the respective absorbances of the samples and standard at the excitation wavelengths, respectively; η^2 and η^2_{Std} are the refractive indices of solvents used for the sample and standard, respectively. 5,10,15,20-tetraphenylporphyrin (TPP) in toluene ($\Phi_F = 0.11$) was used as reference [55].

4.2.2 Singlet oxygen quantum yield

Singlet oxygen formation quantum yields (Φ_Δ) were determined in ethanol and DMSO by direct measurement of singlet oxygen phosphorescence at 1270 nm. The photosensitizer excitation was carried out using the third harmonic of a Spectra-Physics Quanta-Ray GCR-130 Nd–YAG laser (355 nm). Then, the singlet oxygen phosphorescence was collected at 1270 nm using a Hamamatsu R5509-42 photomultiplier cooled to 193 K in a liquid nitrogen chamber. First-degree exponential decay curves of the singlet molecular oxygen emission were extrapolated to time-zero for the reference (phenalenone, $\Phi_\Delta{}^{Std} = 0.97$) [56] and for the samples to obtain a linear relationship between emission intensities and a given laser power. The actual singlet oxygen quantum yields were obtained by comparing this linear dependence between singlet oxygen phosphorescence emission and the energy of the laser pulse for the sample (S) and the reference (S_{Std}) using (2):

$$\Phi_\Delta = \Phi_\Delta^{Std} \frac{S}{1 - 10^{-A}} * \frac{1 - 10^{-A_{Std}}}{S_{Std}} \quad (2)$$

where A and A_{Std} are the absorbance of the sample and the reference, respectively.

4.2.3 Photodegradation studies

The photodegradation studies were conducted in a photosensitizer PBS solution starting with a 0.8–1.0 absorbance in the Soret band. Then, the cuvette was irradiated with a 415 nm light, with light spot with 1 cm diameter and a total power of 0.20 W. A magnetic stirring bar was placed in the cuvette for solution homogenization during irradiation. After each irradiation period, the cuvette was weighted to determine solvent loss due to evaporation. The UV–Visible absorption spectra were recorded before and after each irradiation. The photodegradation quantum yield was calculated following the equation:

$$\Phi_{pd} = \frac{V_d}{V_p} = 0.11978 \times \frac{VA_0k}{\varepsilon \lambda P\left(1 - 10^{-A_i}\right)}$$

were V is the volume of initial solution, A_0 and A_i refer to the initial absorption values at the peak corresponding to the molar absorption coefficient (ε) and the absorption value corresponding to the wavelength of the irradiation light, respectively. P refers to the power of the light [47].

4.2.4 Partition coefficient

The PBS/*n*-octanol partition coefficients (log*P*) were measured following standard methodologies [57]. Approximately, 1 mg of each photosensitizer were first solubilized in 1–2 drops of DMSO and then 5 mL of *n*-octanol, previously saturated with a solution of PBS, and 5 mL of PBS, previously saturaterd with *n*-octanol, were added. Then, the solutions were vigorously shaked and mixed on a vortex and the phases were separated by centrifugation (5 min, 3700 rpm, RT). Next, aliquots from each of the PBS/*n*-octanol phase were taken and diluted to obtain a value of absorption corresponding to Soret band less than 1. The calculation of the partition coefficient was obtained using the following equation:

$$logP = log\left(\frac{Abs_{n-octanol}}{\varepsilon_{n-octanol}}\right) / \left(\frac{Abs_{PBS}}{\varepsilon_{PBS}}\right)$$

4.3 Microbiological studies

4.3.1 Bacterial strains and culture conditions

In this study, we selected a standard *E. coli* strain from American Type Culture Collection (ATCC 25922), that was cultured in Mueller–Hinton broth/agar (Sigma Aldrich).

4.3.2 Light source and illumination conditions

For the photoinactivation studies, a blue LED light ($\lambda = 415$ nm) was used, with a fluence of 6 mW/cm^2. The light dose reported in each experiment represents the actual light dose absorbed by each compound, corrected by LED light emission overlap with compound absorption in water (see Figure S3) [58], using the following multiplicative factors: **IP-H-Me^{2+}** = 0.29; **IP-H-CF3^{2+}** = 0.43; **IP-H-OH^{2+}** = 0.24.

4.3.3 Photoinactivation studies

Stock solutions of each photosensitizer were prepared in DMSO at 1–2 mM concentrations and further diluted with doubly distilled water (ddH_2O) to the desired concentration. The planktonic *E. coli* was cultured in Mueller–Hinton agar (MH) at 37 °C overnight. Cell density was adjusted to the turbidity of the 0.5 McFarland standard in sterile ddH_2O, which corresponds to approximately $1–2 \times 10^8$ CFU/mL. In 96-well plates, 10 µL of the inoculum were added to a solution of 100 µL of photosensitizer (**IP-H-Me^{2+},**

IP-H-CF_3^{2+} or **IP-H-OH^{2+}**) in ddH_2O at the desired concentrations (100 nM and 1 μM), for a final inoculum size of $1–2 \times 10^7$ CFU/mL. The plates were incubated in the dark, at room temperature, for 1 h. Following incubation, the wells were irradiated for a total light dose of 1.36 J/cm^2 light dose. Dark controls were covered in aluminum foil during the time of irradiation. After irradiation, 10 μL aliquots were taken from each well and dilutions in water were done as needed and plated in Petri dishes with MH agar. After 37 °C incubation during 18–24 h, the colony-forming units (CFU) were counted. Experiments were performed in triplicate. In photoinactivation studies where unbound PS was washed, after bacterial dark incubation with the PS, the bacteria suspensions were centrifuged (5000 rpm, 5 min). The supernatant was removed, the bacteria were re-suspended in ddH_2O and the process was repeated two additional times. Then, irradiation was performed under the aforementioned conditions. Data analysis was carried out in GraphPad Prism 8.0 (GraphPad Software, San Diego, California USA).

4.3.4 PS uptake in bacterial cells

Stock solutions of **IP-H-OH^{2+}** and **IP-H-Me^{2+}** were prepared in PBS:DMSO (DMSO 0.5%) and **IP-H-CF_3^{2+}** in PBS:THF (THF 0.5%). The microorganisms were incubated in suspension with a photosensitizer (10 μM) for selected time intervals (0–120 min) in the dark at room temperature. The unbound photosensitizer was removed by washing twice in PBS without Ca^{2+} and Mg^{2+}. After the second wash, bacteria were lysed in 10% SDS for 24 h. The cellular uptake of the photosensitizer was evaluated by determination of fluorescence using excitation at the Soret band and emission between 630–730 nm (Tecan Infinite M200 Reader). Calibration curves were prepared in 10% SDS and used for the determination of PS concentration. Uptake values were obtained by dividing the PS amount (nmol) by the number of CFU.

4.3.5 Flow cytometry studies

Cellular uptake of the investigated photosensitizers was also determined using flow cytometry and quantified based on the red fluorescence of porphyrin. For this analysis, *E. coli* bacteria were incubated with each porphyrin at 10 μM for 2 h. After this incubation, cells were washed two times with PBS without calcium and magnesium ions and collected for analysis. Then, the cells were collected by centrifugation and then resuspended in 200 μL of PBS. Bacteria were then examined using BD Accuri c6 flow cytometer equipped with a red laser (640 nm).

4.3.6 Confocal microscopy studies

Accumulation of the selected porphyrin derivatives in the microorganisms was followed with confocal imaging using a Zeiss LSM880 laser-scanning microscope equipped with an argon-ion laser and the 100 × objective with oil immersion (Carl Zeiss Ltd., Jena, Germany) with a working distance of 1.46 mm. Accordingly, for the uptake studies, bacteria were incubated with the photosensitizer solution (10 μM) for an appropriate time interval determined in the uptake studies (2 h). After washing, the bacteria samples were counterstained with Hoechst33342 (10 μg/mL) for 10 min, placed on the microscopic glass slides, and imaged. Registered images were analyzed with the Zeiss ZEN software.

4.3.7 Combination with cinnamaldehyde

Following the same protocol described in the photoinactivation studies, the bacteria were incubated in the dark for 1 h with 50 nM photosensitizer concentrations an aqueous solution, and then irradiated with 1.36 J/cm^2 at 415 nm. Next, 5 μL of cinnamaldehyde from a DMSO stock solution (150 mM) were added to the bacteria, yielding a 7.5 mM cinnamaldehyde concentration (half of the determined MIC for this strain) in a 5% DMSO aqueous solution. In the control experiment, 5 μL of DMSO (without cinnamaldehyde) were added. The bacteria were incubated for one additional hour in the dark at room temperature, and then 10 μL aliquots were taken from each well and dilutions in water were done as needed and plated in Petri dishes with MH agar. After 37 ºC incubation for 24 h, CFUs were counted. For comparison purposes, monotherapy control experiments were conducted: (i) in PDI monotherapy, 5 μL DMSO (without cinnamaldehyde) was added after treatment and then 10 μL aliquots were plated after 1 h dark incubation; (ii) in cinnamaldehyde monotherapy, bacteria were first irradiated without photosensitizer, then cinnamaldehyde was added and finally 10 μL aliquots were plated after 1 h dark incubation. Experiments were performed in triplicate. Data analysis was carried out in GraphPad Prism 8.0 (GraphPad Software, San Diego, California USA).

4.3.8 In vivo studies

The bacteria were grown in liquid LB medium with shaking at 120 rpm at 37 °C overnight to reach the stationary phase. One mL of this suspension was then refreshed in fresh LB to mid-log phase. Cell numbers were estimated by

measuring the OD at 600 nm. The bacterial suspension was spun down, washed, and resuspended in PBS for the experiments. BALB/c mice, male 8–10-week-old were used for in vivo infection studies. Prior to the experiment, mice were anesthetized by i.p. injection of ketamine/xylazine cocktail. They were shaved using a razor blade on the dorsal surface. A surgical scalpel was used to gently scrape the epidermis off an area of skin to create abrasion wounds. The depth of the wound was no more than the shallow dermis. After creating the wounds, a 50 µL aliquot of bacterial suspension containing 10^7 CFU of fluorescent *E. coli* in PBS was topically inoculated onto each defined area of the abrasion with a pipette tip. Fluorescence images were taken immediately after the inoculation of bacteria to ensure that the number of bacteria applied to each abrasion was consistent. The infection imaging was performed using the NEWTON 7.0 Animal Optical Imaging System (Vilber).

Mice with abrasion wounds infected with *E. coli* were randomly divided into two groups: (1) infection control group and (2) PDT group. The infected abrasion wounds were incubated for 60 min. In the treatment group, a 50 µL aliquot of porphyrin solution (25 µM in a PBS/5% DMSO mixture) was added to the wound and 30 min later the wounds were imaged to quantify any dark toxicity of the porphyrin to the bacteria. Next, the wounds were irradiated with a 420 ± 20 nm light and a total light dose of 120 J/cm^2 (12 min of illumination). Sterile saline (0.5 mL intraperitoneally) was administered to support fluid balance during recovery. For both groups, fluorescence imaging was performed at different time points. To record the time course of the extent of bacterial infection, the bacterial bioluminescence from mouse wounds was measured for 7 days after the wounds until the infections were cured (characterized by the decrease of bacterial fluorescence).

Supplementary Information The online version contains supplementary material available at https://doi.org/10.1007/s43630-024-00581-y.

Acknowledgements This work was funded by FCT—Foundation for Science and Technology, I.P., under projects UIDB/00313/2020, UID/BIA/04004/2020 and PTDC/QUI-OUT/0303/2021. They acknowledge UC-Santander for "PhotoBioSyn" SeedProjects@UC 2024 funding and Project Nº 6979—PRODUTECH R3 [Recuperação-Resiliência-Reindustrialização financed by PRR—Recovery and Resilience Plan and by the Next Generation EU Funds, following Notice n.º 02/C05-i01/2022, Component 5 – Capitalization and Business Innovation—Mobilizing Agendas for Business Innovation. JMD, BP and AB thank National Science Center (NCN), Poland for the Sonata Bis grant no 2016/22/E/NZ7/00420.

Funding Open access funding provided by FCT|FCCN (b-on).

Data availability The datasets generated during and/or analysed during the current study are available from the corresponding author on reasonable request.

Declarations

Conflict of interest The authors have no competing interests to declare that are relevant to the content of this article.

References

1. World Health Organization. (2017). *Global Priority List of Antibiotic Resistant Bacteria to Guide Research, Discovery, and Development of New Antibiotics* (pp. 1–7). World Health Organization.
2. Murray, C. J. L., Ikuta, K. S., Sharara, F., Swetschinski, L., Aguilar, G. R., Gray, A., Han, C., Bisignano, C., Rao, P., Wool, E., Johnson, S. C., Browne, A. J., Chipeta, M. G., Fell, F., Hackett, S., Haines-Woodhouse, G., Hamadani, B. H. K., Kumaran, E. A. P., McManigal, B., et al. (2022). Global burden of bacterial antimicrobial resistance in 2019: A systematic analysis. *Lancet, 399*(10325), 629–655. https://doi.org/10.1016/s0140-6736(21)02724-0
3. Aroso, R. T., Schaberle, F. A., Arnaut, L. G., & Pereira, M. M. (2021). Photodynamic disinfection and its role in controlling infectious diseases. *Photochemical & Photobiological Sciences, 20*(11), 1497–1545. https://doi.org/10.1007/s43630-021-00102-1
4. Cieplik, F., Deng, D., Crielaard, W., Buchalla, W., Hellwig, E., Al-Ahmad, A., & Maisch, T. (2018). Antimicrobial photodynamic therapy—What we know and what we don't. *Critical Reviews in Microbiology, 44*(5), 571–589. https://doi.org/10.1080/1040841X.2018.1467876
5. Nguyen, V. N., Zhao, Z., Tang, B. Z., & Yoon, J. (2022). Organic photosensitizers for antimicrobial phototherapy. *Chemical Society Reviews, 51*(9), 3324–3340. https://doi.org/10.1039/d1cs00647a
6. Hamblin, M. R., & Jori, G. (2011). *Photodynamic Inactivation of Microbial Pathogens*. The Royal Society of Chemistry.
7. Warrier, A., Mazumder, N., Prabhu, S., Satyamoorthy, K., & Murali, T. S. (2021). Photodynamic therapy to control microbial biofilms. *Photodiagnosis and Photodynamic Therapy, 33*, 102090. https://doi.org/10.1016/j.pdpdt.2020.102090
8. Vinagreiro, C. S., Zangirolami, A., Schaberle, F. A., Nunes, S. C. C., Blanco, K. C., Inada, N. M., da Silva, G. J., Pais, A., Bagnato, V. S., Arnaut, L. G., & Pereira, M. M. (2020). Antibacterial photodynamic inactivation of antibiotic-resistant bacteria and biofilms with nanomolar photosensitizer concentrations. *ACS Infectious Diseases, 6*(6), 1517–1526. https://doi.org/10.1021/acsinfecdis.9b00379
9. Hu, X., Huang, Y. Y., Wang, Y., Wang, X., & Hamblin, M. R. (2018). Antimicrobial photodynamic therapy to control clinically relevant biofilm infections. *Frontiers in Microbiology, 9*, 1299. https://doi.org/10.3389/fmicb.2018.01299
10. Xuan, W., Huang, L., Wang, Y., Hu, X., Szewczyk, G., Huang, Y. Y., El-Hussein, A., Bommer, J. C., Nelson, M. L., Sarna, T.,

& Hamblin, M. R. (2019). Amphiphilic tetracationic porphyrins are exceptionally active antimicrobial photosensitizers: In vitro and in vivo studies with the free-base and Pd-chelate. *Journal of Biophotonics, 12*(8), e201800318. https://doi.org/10.1002/jbio.201800318

11. Alenezi, K., Tovmasyan, A., Batinic-Haberle, I., & Benov, L. T. (2017). Optimizing Zn porphyrin-based photosensitizers for efficient antibacterial photodynamic therapy. *Photodiagnosis and Photodynamic Therapy, 17*, 154–159. https://doi.org/10.1016/j.pdpdt.2016.11.009
12. Marciel, L., Mesquita, M. Q., Ferreira, R., Moreira, B., Neves, P. M. S., Faustino, M. A. F., & Almeida, A. (2018). An efficient formulation based on cationic porphyrins to photoinactivate *Staphylococcus aureus* and *Escherichia coli*. *Future Medicinal Chemistry, 10*(15), 1821–1833. https://doi.org/10.4155/fmc-2018-0010
13. Caruso, E., Malacarne, M. C., Banfi, S., Gariboldi, M. B., & Orlandi, V. T. (2019). Cationic diarylporphyrins: In vitro versatile anticancer and antibacterial photosensitizers. *Journal of Photochemistry and Photobiology B: Biology, 197*, 111548. https://doi.org/10.1016/j.jphotobiol.2019.111548
14. Sulek, A., Pucelik, B., Kobielusz, M., Barzowska, A., & Dabrowski, J. M. (2020). Photodynamic inactivation of bacteria with porphyrin derivatives: Effect of charge, lipophilicity, ROS generation, and cellular uptake on their biological activity in vitro. *International Journal of Molecular Sciences, 21*(22), 8716. https://doi.org/10.3390/ijms21228716
15. Ziganshyna, S., Guttenberger, A., Lippmann, N., Schulz, S., Bercker, S., Kahnt, A., Ruffer, T., Voigt, A., Gerlach, K., & Werdehausen, R. (2020). Tetrahydroporphyrin-tetratosylate (THPTS)-based photodynamic inactivation of critical multidrug-resistant bacteria in vitro. *International Journal of Antimicrobial Agents, 55*(6), 105976. https://doi.org/10.1016/j.ijantimicag.2020.105976
16. Almeida, J., Tome, J. P., Neves, M. G., Tome, A. C., Cavaleiro, J. A., Cunha, A., Costa, L., Faustino, M. A., & Almeida, A. (2014). Photodynamic inactivation of multidrug-resistant bacteria in hospital wastewaters: Influence of residual antibiotics. *Photochemical & Photobiological Sciences, 13*(4), 626–633. https://doi.org/10.1039/c3pp50195g
17. Merchat, M., Bertolini, G., Giacomini, P., Villaneuva, A., & Jori, G. (1996). Meso-substituted cationic porphyrins as efficient photosensitizers of gram-positive and gram-negative bacteria. *Journal of Photochemistry and Photobiology B: Biology, 32*(3), 153–157. https://doi.org/10.1016/1011-1344(95)07147-4
18. Banfi, S., Caruso, E., Buccafurni, L., Battini, V., Zazzaron, S., Barbieri, P., & Orlandi, V. (2006). Antibacterial activity of tetraaryl-porphyrin photosensitizers: An in vitro study on Gram negative and Gram positive bacteria. *Journal of Photochemistry and Photobiology B: Biology, 85*(1), 28–38. https://doi.org/10.1016/j.jphotobiol.2006.04.003
19. Salmon-Divon, M., Nitzan, Y., & Malik, Z. (2004). Mechanistic aspects of Escherichia coli photodynamic inactivation by cationic tetra-meso(N-methylpyridyl)porphine. *Photochemical & Photobiological Sciences, 3*(5), 423–429. https://doi.org/10.1039/B315627N
20. Orlandi, V. T., Caruso, E., Tettamanti, G., Banfi, S., & Barbieri, P. (2013). Photoinduced antibacterial activity of two dicationic 5,15-diarylporphyrins. *Journal of Photochemistry and Photobiology B: Biology, 127*, 123–132. https://doi.org/10.1016/j.jphotobiol.2013.08.011
21. Ragàs, X., Agut, M., & Nonell, S. (2010). Singlet oxygen in Escherichia coli: New insights for antimicrobial photodynamic therapy. *Free Radical Biology and Medicine, 49*(5), 770–776. https://doi.org/10.1016/j.freeradbiomed.2010.05.027
22. Hurst, A. N., Scarbrough, B., Saleh, R., Hovey, J., Ari, F., Goyal, S., Chi, R. J., Troutman, J. M., & Vivero-Escoto, J. L. (2019). Influence of cationic meso-substituted porphyrins on the antimicrobial photodynamic efficacy and cell membrane interaction in *Escherichia coli*. *International Journal of Molecular Sciences, 20*(1), 134. https://doi.org/10.3390/ijms20010134
23. Cormick, M. P., Alvarez, M. G., Rovera, M., & Durantini, E. N. (2009). Photodynamic inactivation of Candida albicans sensitized by tri- and tetra-cationic porphyrin derivatives. *European Journal of Medicinal Chemistry, 44*(4), 1592–1599. https://doi.org/10.1016/j.ejmech.2008.07.026
24. Gsponer, N. S., Spesia, M. B., & Durantini, E. N. (2015). Effects of divalent cations, EDTA and chitosan on the uptake and photoinactivation of Escherichia coli mediated by cationic and anionic porphyrins. *Photodiagnosis and Photodynamic Therapy, 12*(1), 67–75. https://doi.org/10.1016/j.pdpdt.2014.12.004
25. Aroso, R. T., Calvete, M. J. F., Pucelik, B., Dubin, G., Arnaut, L. G., Pereira, M. M., & Dabrowski, J. M. (2019). Photoinactivation of microorganisms with sub-micromolar concentrations of imidazolium metallophthalocyanine salts. *European Journal of Medical Chemistry, 184*, 111740. https://doi.org/10.1016/j.ejmech.2019.111740
26. Aroso, R. T., Dias, L. D., Blanco, K. C., Soares, J. M., Alves, F., Silva, G. J., Arnaut, L. G., Bagnato, V. S., & Pereira, M. M. (2022). Synergic dual phototherapy: Cationic imidazolyl photosensitizers and ciprofloxacin for eradication of in vitro and in vivo *E. coli* infections. *Journal of Photochemistry and Photobiology B: Biology, 233*, 112499. https://doi.org/10.1016/j.jphotobiol.2022.112499
27. Wozniak, A., & Grinholc, M. (2018). Combined antimicrobial activity of photodynamic inactivation and antimicrobials-state of the art. *Frontiers in Microbiology, 9*, 930. https://doi.org/10.3389/fmicb.2018.00930
28. Morley, S., Griffiths, J., Philips, G., Moseley, H., O'Grady, C., Mellish, K., Lankester, C. L., Faris, B., Young, R. J., Brown, S. B., & Rhodes, L. E. (2013). Phase IIa randomized, placebo-controlled study of antimicrobial photodynamic therapy in bacterially colonized, chronic leg ulcers and diabetic foot ulcers: A new approach to antimicrobial therapy. *British Journal of Dermatology, 168*(3), 617–624. https://doi.org/10.1111/bjd.12098
29. Mannucci, E., Genovese, S., Monami, M., Navalesi, G., Dotta, F., Anichini, R., Romagnoli, F., & Gensini, G. (2014). Photodynamic topical antimicrobial therapy for infected foot ulcers in patients with diabetes: A randomized, double-blind, placebo-controlled study – The D.A.N.T.E (Diabetic ulcer Antimicrobial New Topical treatment Evaluation) study. *Acta Diabetologica, 51*(3), 435–440. https://doi.org/10.1007/s00592-013-0533-3
30. Hamblin, M. R., O'Donnell, D. A., Murthy, N., Contag, C. H., & Hasan, T. (2007). Rapid control of wound infections by targeted photodynamic therapy monitored by in vivo bioluminescence imaging. *Photochemistry and Photobiology, 75*(1), 51–57. https://doi.org/10.1562/0031-8655(2002)0750051rcowib2.0.Co2
31. Dai, T., Tegos, G. P., Zhiyentayev, T., Mylonakis, E., & Hamblin, M. R. (2010). Photodynamic therapy for methicillin-resistant *Staphylococcus aureus* infection in a mouse skin abrasion model. *Lasers in Surgery and Medicine, 42*(1), 38–44. https://doi.org/10.1002/lsm.20887
32. Mai, B., Gao, Y., Li, M., Wang, X., Zhang, K., Liu, Q., Xu, C., & Wang, P. (2017). Photodynamic antimicrobial chemotherapy for *Staphylococcus aureus* and multidrug-resistant bacterial burn infection in vitro and in vivo. *International Journal of Nanomedicine, 12*, 5915–5931. https://doi.org/10.2147/IJN.S138185

33. Soares, J. M., Guimarães, F. E. G., Yakovlev, V. V., Bagnato, V. S., & Blanco, K. C. (2022). Physicochemical mechanisms of bacterial response in the photodynamic potentiation of antibiotic effects. *Scientific Reports, 12*(1), 21146. https://doi.org/10.1038/s41598-022-25546-y
34. Soares, J. M., Yakovlev, V. V., Blanco, K. C., & Bagnato, V. S. (2023). Recovering the susceptibility of antibiotic-resistant bacteria using photooxidative damage. *Proceedings of the National Academy of Sciences, 120*(39), e2311667120. https://doi.org/10.1073/pnas.2311667120
35. Pérez-Laguna, V., Gilaberte, Y., Millán-Lou, M. I., Agut, M., Nonell, S., Rezusta, A., & Hamblin, M. R. (2019). A combination of photodynamic therapy and antimicrobial compounds to treat skin and mucosal infections: A systematic review. *Photochemical & Photobiological Sciences, 18*(5), 1020–1029. https://doi.org/10.1039/c8pp00534f
36. Feng, Y., Coradi Tonon, C., Ashraf, S., & Hasan, T. (2021). Photodynamic and antibiotic therapy in combination against bacterial infections: Efficacy, determinants, mechanisms, and future perspectives. *Advanced Drug Delivery Reviews, 177*, 113941. https://doi.org/10.1016/j.addr.2021.113941
37. Aroso, R. T., Piccirillo, G., Dias, L. D., Pinto, S. M. A., Arnaut, L. G., & Pereira, M. M. (2022). Synthesis of photosensitizers based on tetrapyrrolic macrocycles for combination with antibiotics: Dual inactivation of bacteria. *ChemPlusChem, 87*(11), e202200228. https://doi.org/10.1002/cplu.202200228
38. Doyle, A. A., & Stephens, J. C. (2019). A review of cinnamaldehyde and its derivatives as antibacterial agents. *Fitoterapia, 139*, 104405. https://doi.org/10.1016/j.fitote.2019.104405
39. IFRA Standard - Cinnamic aldehyde (2023). https://ifrafragrance.org/standards/IFRA_STD48_0168.pdf Accessed 28 Dec 2023
40. Pang, D., Huang, Z., Li, Q., Wang, E., Liao, S., Li, E., Zou, Y., & Wang, W. (2021). Antibacterial mechanism of cinnamaldehyde: Modulation of biosynthesis of phosphatidylethanolamine and phosphatidylglycerol in *Staphylococcus aureus* and *Escherichia coli*. *Journal of Agricultural and Food Chemistry, 69*(45), 13628–13636. https://doi.org/10.1021/acs.jafc.1c04977
41. Friedman, M. (2017). Chemistry, antimicrobial mechanisms, and antibiotic activities of cinnamaldehyde against pathogenic bacteria in animal feeds and human foods. *Journal of Agricultural and Food Chemistry, 65*(48), 10406–10423. https://doi.org/10.1021/acs.jafc.7b04344
42. Shen, S., Zhang, T., Yuan, Y., Lin, S., Xu, J., & Ye, H. (2015). Effects of cinnamaldehyde on *Escherichia coli* and *Staphylococcus aureus* membrane. *Food Control, 47*, 196–202. https://doi.org/10.1016/j.foodcont.2014.07.003
43. Arnaut, Z. A., Pinto, S. M. A., Aroso, R. T., Amorim, A. S., Lobo, C. S., Schaberle, F. A., Pereira, D., Nunez, J., Nunes, S. C. C., Pais, A., Rodrigues-Santos, P., de Almeida, L. P., Pereira, M. M., & Arnaut, L. G. (2023). Selective, broad-spectrum antiviral photodynamic disinfection with dicationic imidazolyl chlorin photosensitizers. *Photochemical & Photobiological Sciences, 22*, 2607–2620. https://doi.org/10.1007/s43630-023-00476-4
44. Ruani, F., Edo-Osagie, A., Rouville, H.-P.J., Heitz, V., Ventura, B., & Armaroli, N. (2023). Photophysical characterization of a bisacridinium-diphenylporphyrin conjugate. *Journal of Porphyrins and Phthalocyanines, 27*(0104), 569–575. https://doi.org/10.1142/s1088424623500396
45. Caminos, D. A., Spesia, M. B., & Durantini, E. N. (2006). Photodynamic inactivation of Escherichia coli by novel meso-substituted porphyrins by 4-(3-N, N, N-trimethylammoniumpropoxy) phenyl and 4-(trifluoromethyl)phenyl groups. *Photochemical & Photobiological Sciences, 5*(1), 56–65. https://doi.org/10.1039/B513511G
46. Merchat, M., Spikes, J. D., Bertoloni, G., & Jori, G. (1996). Studies on the mechanism of bacteria photosensitization by meso-substituted cationic porphyrins. *Journal of Photochemistry and Photobiology B: Biology, 35*(3), 149–157. https://doi.org/10.1016/S1011-1344(96)07321-6
47. Arnaut, L. G., Pereira, M. M., Dąbrowski, J. M., Silva, E. F. F., Schaberle, F. A., Abreu, A. R., Rocha, L. B., Barsan, M. M., Urbańska, K., Stochel, G., & Brett, C. M. A. (2014). Photodynamic therapy efficacy enhanced by dynamics: the role of charge transfer and photostability in the selection of photosensitizers. *Chemistry—A European Journal, 20*(18), 5346–5357. https://doi.org/10.1002/chem.201304202
48. Bonnett, R., & Martínez, G. (2001). Photobleaching of sensitisers used in photodynamic therapy. *Tetrahedron, 57*(47), 9513–9547. https://doi.org/10.1016/s0040-4020(01)00952-8
49. Slomp, A. M., Barreira, S. M. W., Carrenho, L. Z. B., Vandresen, C. C., Zattoni, I. F., Ló, S. M. S., Dallagnol, J. C. C., Ducatti, D. R. B., Orsato, A., Duarte, M. E. R., Noseda, M. D., Otuki, M. F., & Gonçalves, A. G. (2017). Photodynamic effect of meso-(aryl)porphyrins and meso-(1-methyl-4-pyridinium)porphyrins on HaCaT keratinocytes. *Bioorganic & Medicinal Chemistry Letters, 27*(2), 156–161. https://doi.org/10.1016/j.bmcl.2016.11.094
50. Yu, C., Li, Y. L., Liang, M., Dai, S. Y., Ma, L., Li, W. G., Lai, F., & Liu, X. M. (2020). Characteristics and hazards of the cinnamaldehyde oxidation process. *RSC Advances, 10*(32), 19124–19133. https://doi.org/10.1039/c9ra10820c
51. Chen, H., Ji, H., Zhou, X., Xu, J., & Wang, L. (2009). Aerobic oxidative cleavage of cinnamaldehyde to benzaldehyde catalyzed by metalloporphyrins under mild conditions. *Catalysis Communications, 10*(6), 828–832. https://doi.org/10.1016/j.catcom.2008.12.007
52. Garcez, A. S., Kaplan, M., Jensen, G. J., Scheidt, F. R., Oliveira, E. M., & Suzuki, S. S. (2020). Effects of antimicrobial photodynamic therapy on antibiotic-resistant *Escherichia coli*. *Photodiagnosis and Photodynamic Therapy, 32*, 102029. https://doi.org/10.1016/j.pdpdt.2020.102029
53. Albano, M., Crulhas, B. P., Alves, F. C. B., Pereira, A. F. M., Andrade, B., Barbosa, L. N., Furlanetto, A., Lyra, L., Rall, V. L. M., & Junior, A. F. (2019). Antibacterial and anti-biofilm activities of cinnamaldehyde against *S. epidermidis*. *Microbial Pathogenesis, 126*, 231–238. https://doi.org/10.1016/j.micpath.2018.11.009
54. Vecchio, D., Gupta, A., Huang, L., Landi, G., Avci, P., Rodas, A., & Hamblin, M. R. (2015). Bacterial photodynamic inactivation mediated by methylene blue and red light is enhanced by synergistic effect of potassium iodide. *Antimicrobial Agents & Chemotherapy, 59*(9), 5203–5212. https://doi.org/10.1128/AAC.00019-15
55. Pineiro, M., Carvalho, A. L., Pereira, M. M., Gonsalves, A. M. A. R., & ArnautFormosinho, L. G. S. J. (1998). Photoacoustic measurements of porphyrin triplet-state quantum yields and singlet-oxygen efficiencies. *Chemistry—A European Journal, 4*(11), 2299–2307. https://doi.org/10.1002/(SICI)1521-3765(19981102)4:11%3c2299::AID-CHEM2299%3e3.0.CO;2-H
56. Schmidt, R., Tanielian, C., Dunsbach, R., & Wolff, C. (1994). Phenalenone, a universal reference compound for the determination of quantum yields of singlet oxygen O2(1Δg) sensitization. *Journal of Photochemistry and Photobiology A: Chemistry, 79*(1), 11–17. https://doi.org/10.1016/1010-6030(93)03746-4
57. Baláž, Š. (2000). Lipophilicity in trans-bilayer transport and subcellular pharmacokinetics. *Perspectives in Drug Discovery and Design, 19*(1), 157–177. https://doi.org/10.1023/A:1008775707749
58. Schaberle, F. A. (2018). Assessment of the actual light dose in photodynamic therapy. *Photodiagnosis and Photodynamic Therapy, 23*, 75–77. https://doi.org/10.1016/j.pdpdt.2018.06.009

Authors and Affiliations

Madalena F. C. Silva[1] · Rafael T. Aroso[1] · Janusz M. Dabrowski[2] · Barbara Pucelik[3] · Agata Barzowska[3] · Gabriela J. da Silva[4] · Luis G. Arnaut[1] · Mariette M. Pereira[1]

✉ Rafael T. Aroso
rafaelaroso@uc.pt

✉ Janusz M. Dabrowski
jdabrows@chemia.uj.edu.pl

✉ Mariette M. Pereira
mmpereira@qui.uc.pt

[1] Department of Chemistry, CQC-IMS, University of Coimbra, 3004-535 Coimbra, Portugal

[2] Faculty of Chemistry, Jagiellonian University, Gronostajowa 2, 30-387 Krakow, Poland

[3] Malopolska Center of Biotechnology, Jagiellonian University, Gronostajowa 7A, 30-387 Krakow, Poland

[4] Faculty of Pharmacy and Center for Neurosciences and Cell Biology, University of Coimbra, Azinhaga de Santa Comba, 3000-548 Coimbra, Portugal